Chemistry & Biology
Article

Functional Plasticity and Allosteric Regulation of α-Ketoglutarate Decarboxylase in Central Mycobacterial Metabolism

Tristan Wagner,[1] Marco Bellinzoni,[1] Annemarie Wehenkel,[1,3] Helen M. O'Hare,[2,*] and Pedro M. Alzari[1,*]
[1]Institut Pasteur, Unité de Biochimie Structurale (CNRS URA 2185), 25 rue du Dr. Roux, 75724 Paris, France
[2]Department of Infection, Immunity and Inflammation, University of Leicester, University Road, LE1 9HN Leicester, UK
[3]Present address: Max-Planck-Institute for Molecular Physiology, 11 Otto-Hahn Strasse, 44227 Dortmund, Germany
*Correspondence: hmo7@leicester.ac.uk (H.M.O.), pedro.alzari@pasteur.fr (P.M.A.)
DOI 10.1016/j.chembiol.2011.06.004

SUMMARY

The α-ketoglutarate dehydrogenase (KDH) complex is a major regulatory point of aerobic energy metabolism. *Mycobacterium tuberculosis* was reported to lack KDH activity, and the putative KDH E1o component, α-ketoglutarate decarboxylase (KGD), was instead assigned as a decarboxylase or carboligase. Here, we show that this protein does in fact sustain KDH activity, as well as the additional two reactions, and these multifunctional properties are shared by the *Escherichia coli* homolog, SucA. We also show that the mycobacterial enzyme is finely regulated by an additional acyltransferase-like domain and by the action of acetyl-CoA, a powerful allosteric activator able to enhance the concerted protein motions observed during catalysis. Our results uncover the functional plasticity of a crucial node in bacterial metabolism, which may be important for *M. tuberculosis* during host infection.

INTRODUCTION

The tricarboxylic acid (TCA) cycle catalyzes the total oxidation of acetyl units derived from other catabolic pathways and is the major energy-generating pathway in aerobic organisms. Within the cycle the α-ketoglutarate dehydrogenase (KDH) complex plays an important regulatory role, catalyzing a high-flux reaction at the branch point between energy production and nitrogen metabolism (Bunik and Fernie, 2009). In addition to energy metabolism, the TCA cycle is a major source of biosynthetic precursors, which may be obtained by noncyclic flux, with oxidative and reducing branches leading respectively to α-ketoglutarate (KG) and succinate (Guest, 1995). Noncyclic flux is characterized by the absence (or repression) of the KG dehydrogenase (KDH) complex. Some microaerophilic or anaerobic bacteria directly lack KDH genes, such as *Helicobacter pylori* (Tomb et al., 1997), in which the oxidative and reductive branches are linked by KG oxidase (KGO) activity (Pitson et al., 1999), whereas others, like *Escherichia coli*, operate a complete TCA cycle aerobically but can repress KDH under anaerobic conditions (Keevil et al., 1979).

Mycobacterium tuberculosis (*Mtb*), the etiological agent of tuberculosis, can survive for long periods in a hypoxic environment (Wayne and Hayes, 1996) but is generally considered a strictly aerobic bacillus and has functional genes coding for all enzymes of the standard TCA cycle (Cole et al., 1998; Murthy et al., 1962). Thus, although the presence of a functional glyoxylate shunt (McKinney et al., 2000) and an anaerobic-like KG:ferredoxin oxidoreductase (KGO) (Baughn et al., 2009) could bypass the requirement for KDH activity, it is, nevertheless, intriguing that mycobacteria were reported to lack a functional KDH complex (Tian et al., 2005b), given the enormous energetic benefits of aerobic respiration and the oxidative environment in many sites of infection, such as the lung and macrophages. Instead, the putative E1o component of the KDH complex was characterized as a thiamine diphosphate (ThDP)-dependent KG decarboxylase (KGD) to produce succinic semialdehyde (SSA) (Tian et al., 2005b) and more recently as an efficient carboligase on glyoxylate (de Carvalho et al., 2010).

Here, we report structural and biochemical studies of *Mycobacterium smegmatis* KGD (*Ms*KGD) and the *Mtb* homolog, Rv1248c, demonstrating that KGD is a multifunctional enzyme capable of sustaining succinyl-transferring KDH activity, in addition to the reported KGD and carboligase activities. Furthermore, this multifunctionality is not a unique feature of the mycobacterial enzyme because the *E. coli* E1o homolog SucA (*Ec*SucA) was also found to efficiently catalyze all three reactions. However, mycobacterial KGD has low basal activities, which might account at least in part for previous failures in detecting KDH activity in mycobacteria, and we show here that the enzyme requires specific activation by acetyl-CoA, the main substrate of the TCA cycle, to achieve specific activities comparable to those of *Ec*SucA. The active site architecture of *Ms*KGD is shown to undergo a considerable structural rearrangement during the catalytic cycle. Acetyl-CoA binds to an allosteric site 40 Å away from the catalytic center and stimulates *Ms*KGD activity by promoting local conformational changes that facilitate formation of the enamine-ThDP reaction intermediate. Taken together, our results uncover the functional versatility of KGD in bacterial metabolism and highlight the presence of three alternative, tightly regulated, pathways connecting the oxidative and reductive branches of the TCA cycle in *Mtb*, whose differential utilization may provide an advantage for pathogen growth within its human host.

Table 1. Crystallographic Data Collection and Refinement Statistics

	$KGD_{\Delta360}$	$KGD_{\Delta115}$	$KGD_{\Delta360}$ Enamine-ThDP Intermediate	$KGD_{\Delta360}$-AcCoA	$KGD_{\Delta360}$ Enamine-ThDP Intermediate-AcCoA
Data Collection					
Synchrotron beamline	ESRF ID14-4	SOLEIL Proxima 1	SOLEIL Proxima 1	SLS X06DA	SOLEIL Proxima 1
Wavelength (Å)	0.9765	1.0332	0.9801	0.9801	0.9801
Space group	P1	$P2_12_12$	P1	P1	P1
Cell dimensions					
a, *b*, *c* (Å)	79.54, 83.24, 158.61	79.98, 151.99, 242.72	79.84, 82.29, 163.48	80.50, 83.32, 159.92	81.06, 81.95, 161.88
α, β, γ (°)	99.5, 99.1, 101.3	90.0, 90.0, 90.0	99.2, 99.0, 100.6	99.6, 99.0, 100.7	99.3, 97.1, 100.6
Resolution (Å)	49.5–1.96 (2.07–1.96)	82–2.74 (2.89–2.74)	41.9–2.25 (2.37–2.25)	78.1–2.2 (2.31–2.2)	41.4–2.40 (2.53–2.40)
R_{sym} or R_{merge}	0.089 (0.445)	0.074 (0.416)	0.101 (0.481)	0.067 (0.395)	0.105 (0.562)
$I/\sigma(I)$	8.7 (2.2)	10.3 (2.4)	6.9 (2.0)	8.7 (2.2)	7.4 (1.9)
Completeness (%)	95.2 (91.5)	99.3 (97.5)	95.7 (94.6)	92.6 (88.5)	95.8 (95.6)
Redundancy	2.9 (2.4)	3.5 (3.2)	2.0 (1.9)	2.0 (2.0)	2.5 (2.4)
Refinement					
Resolution (Å)	1.96	2.74	2.25	2.20	2.40
Number of reflections	263,738	79,835	179,896	187,791	149,475
R_{work}/R_{free} (%)	18.8/21.1	18.5/22.4	19.2/22.3	18.8/21.4	19.7/22.0
Number of atoms					
Protein	25,030	15,727	26,117	25,144	25,968
Ligand/ion	112	56	140	211	327
Water	1,221	119	730	742	514
B factors					
Protein	29.0	70.3	33.8	44.1	45.1
Ligand/ion	16.8	49.0	23.0	46.5	41.6
Water	26.8	50.5	26.8	34.3	32.1
Rms deviations					
Bond lengths (Å)	0.010	0.010	0.010	0.010	0.008
Bond angles (°)	0.98	1.09	1.01	1.02	0.97

Highest resolution shell is shown in parenthesis.

RESULTS AND DISCUSSION

Overall Structure of Mycobacterial KGD

Extensive screening for crystallization conditions of full-length *Ms*KGD resulted in low-resolution diffracting crystals, which were not exploitable for structural studies. Treatment of the enzyme with proteases led to the rapid excision of the first 115 amino acid residues from the N terminus (see Figure S1A available online), suggesting that this region is unstructured in the native protein and might hinder crystallization. Consequently, the structure of a truncated form of the enzyme lacking this N-terminal region ($MsKGD_{\Delta115}$) was determined at 2.74 Å resolution (Table 1). The protein is a homodimer, in which each subunit is composed of several distinct domains (Figure 1A). The N-terminal domain (residues 116–360), which was originally identified in the *Corynebacterium glutamicum* homolog OdhA (Usuda et al., 1996), is only found in corynebacterineae enzymes but is missing in other bacterial E1o homologs, such as *Ec*SucA. This domain folds into a two-layered open-faced sandwich motif structurally similar to the subunit fold of trimeric acyltransferases (Knapp et al., 2000), and was shown to encode the succinyltransferase (E2o) activity in *C. glutamicum* OdhA (Hoffelder et al., 2010). The rest of the subunit displays a similar quaternary organization to that described for *Ec*SucA (Figure S1B), the only other E1o component, to our knowledge, for which a crystal structure is currently available (Frank et al., 2007). In *Ms*KGD the acyltransferase domain is connected to (and interacts extensively with) a small helical domain (*Ms*KGD residues 361–445) involved in protein dimerization, followed by three consecutive α/β domains (residues 446–814, 831–1091, and 1092–1227) displaying the characteristic fold of ThDP-dependent enzymes (Figure 1A). First described for transketolase (Lindqvist et al., 1992), this common fold was subsequently found in other homodimeric dehydrogenases (Muller et al., 1993) as well as in heterotetrameric enzymes such as eukaryotic pyruvate dehydrogenases (PDHs), in which the basic subunit lacks an interdomain linker connecting the first and second α/β domains and is encoded by two different polypeptides. In the structure of the $MsKGD_{\Delta115}$ homodimer, the equivalent connecting linker (residues 810–830) is disordered (Figure 1A) and presumably adopts a flexible conformation.

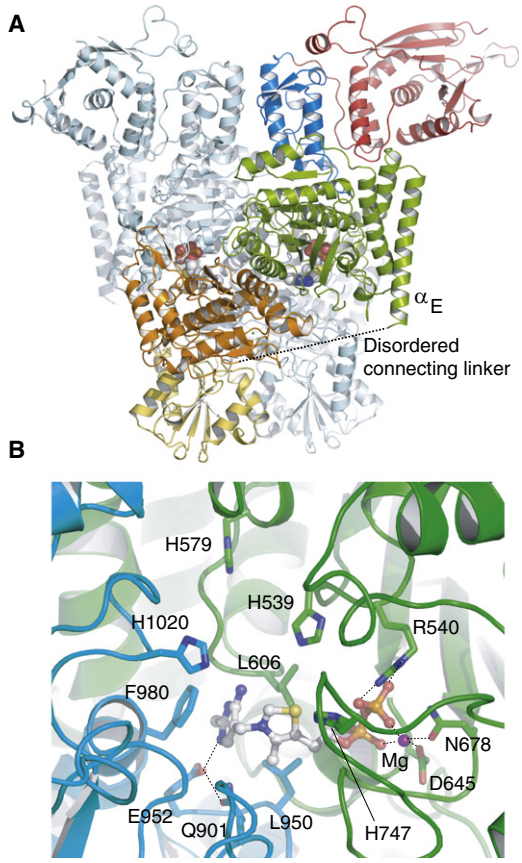

Figure 1. Overall Structure of *Ms*KGD

(A) Cartoon representation of the *Ms*KGD$_{\Delta 115}$ homodimer. Each subunit consists of an acyltransferase-like domain (shown in red), a small helical domain (blue), and three consecutive α/β domains (green, orange, and yellow, respectively). An interdomain linker (residues 810–830, disordered in the crystal structure) connects an external helix (labeled α_E) at the end of the first α/β domain with the N terminus of the second α/β domain ~60 Å apart.

(B) Close view of the catalytic site around the ThDP cofactor. See also Figure S1 and Table S1.

The functional dimeric arrangement, common to all ThDP-dependent enzymes (Muller et al., 1993), is conserved in *Ms*KGD. The ThDP cofactor is bound in a cleft between the two subunits (Figure 1B). The diphosphate moiety of the cofactor interacts primarily with one of the monomers and is stabilized through hydrogen bonds to the guanidine group of Arg540 and, via the Mg^{2+} ion, to the polar side chains of Asn678 and Asp645. The thiazolium ring is located between the subunits, where hydrophobic interactions with Leu606 and Leu950 (from different subunits) stabilize the V-shape conformation of the cofactor required for intramolecular proton transfer (Nemeria et al., 2007). The pyrimidine ring makes stacking interactions with the phenyl group of Phe980, and the N1 atom from this ring is hydrogen bonded to the carboxylate group of Glu952, a crucial interaction for ThDP activation. Positioned in the proximity of the catalytic site (Figure 1B), four histidine residues (His539, His579, His747, and His1020) play important roles in substrate binding or catalysis because their substitution by alanine significantly decreased or abolished decarboxylase activity (Table S1). All the aforementioned residues, mediating ThDP/substrate binding or involved in catalysis, are largely invariant in both corynebacterineae enzymes (KGD/OdhA) as well as in bacterial SucA homologs. These observations, together with the substantial similarities in overall fold and active site architecture, argue against the reported functional differences between mycobacterial KGD and other SucA homologs, prompting us to reinvestigate their enzymatic properties.

Mycobacterial KGD and *E. coli* SucA Are Multifunctional Enzymes

As reported for the *Mtb* enzyme (de Carvalho et al., 2010; Tian et al., 2005a), we found that *Ms*KGD (with or without the N-terminal acyltransferase-like domain) efficiently catalyzed the oxidative decarboxylation of KG into SSA as well as the synthesis of 2-hydroxy-3-oxoadipate in the presence of glyoxylate (Figure 2A). Importantly, the succinyl-transferring KDH from *E. coli*, *Ec*SucA (Waskiewicz and Hammes, 1984), was also found to efficiently catalyze both the decarboxylase and carboligase reactions (Figure 2A), suggesting that multifunctionality of the ThDP-dependent catalytic site is a general feature of bacterial KGD/SucA homologs, independently of the presence (KGD) or absence (SucA) of the N-terminal acyltransferase-like domain. To our knowledge, no carboligase or decarboxylase activities had been previously reported for the E1o component of the *E. coli* KDH complex. Nevertheless, our findings are consistent with the biochemical detection of these different ThDP-dependent activities in cell extracts from a number of bacterial species, including *E. coli* and mycobacteria (Yamasaki and Moriyama, 1970, 1971), and can also account for early reports describing multiple activities associated with bacterial and mammalian KDH complexes (Bunik and Fernie, 2009; O'Fallon and Brosemer, 1977; Schlossberg et al., 1970).

The FHA domain-containing protein GarA has been recently identified as a phospho-dependent regulator of metabolic enzymes (including KGD) involved in glutamate synthesis under control of the Ser/Thr protein kinase PknG in both corynebacteria and mycobacteria (Niebisch et al., 2006; Bott, 2007; O'Hare et al., 2008; Nott et al., 2009). As expected, the GarA FHA domain strongly inhibited *Ms*KGD, whereas it had no effect on *Ec*SucA (Figure 2B). Furthermore, GarA is able to inhibit not only full-length *Ms*KGD but also the shorter constructs *Ms*KGD$_{\Delta 115}$ and *Ms*KGD$_{\Delta 360}$, indicating that the FHA domain binds to the C-terminal catalytic core of KGD, as recently reported for the *C. glutamicum* KGD homolog, OdhA (Krawczyk et al., 2010).

Acetyl-CoA Is a Potent Activator of Mycobacterial KGD

Mycobacterial KGD displays unique regulatory properties, which are possibly linked to the presence of the additional N-terminal acyltransferase-like domain. Indeed, the shorter construct *Ms*KGD$_{\Delta 360}$ (comprising the region equivalent to *Ec*SucA but lacking the N-terminal domain) was found to be significantly more efficient in SSA production than *Ms*KGD$_{\Delta 115}$ or full-length *Ms*KGD (Figure 2B), denoting a partial inhibitory role of the acyltransferase-like domain in full-length KGD. The N-terminal domain interacts with the catalytic core through an extended (~1400 $Å^2$) intrasubunit interface involving several polar and hydrophobic contacts (Figure S1C). To investigate whether this interaction could promote structural modifications accounting

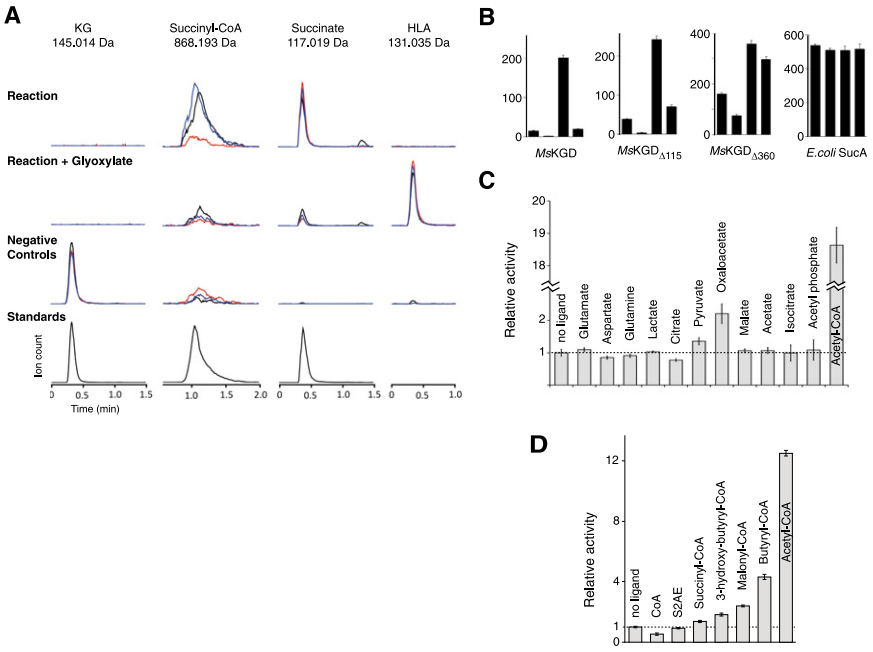

Figure 2. Enzymatic Activities of *Ms*KGD and *Ec*SucA

(A) LC-MS analysis of the products of *Ms*KGD (blue), *Ms*KGD$_{\Delta 360}$ (red), and *Ec*SucA (black). The product of the KDH reaction (succinyl-CoA) was directly detected, whereas the products of the KGD (SSA) and carboligase (2-hydroxy-3-oxoadipate, HOA) reactions were converted to succinate and 5-hydroxylevulinate (HLA), respectively, for detection. Negative controls: – Mg, – ThDP, + inhibitory protein GarA.

(B) Specific KGD activities measured by coupled assay with SSA dehydrogenase (nmol of NADPH product/min/mg) of different proteins, alone (first bar) and in presence of 5 μM GarA FHA domain (second bar), 1 mM acetyl-CoA (third bar), or both (fourth bar). Error bars represent the standard deviation from three independent experiments.

(C) Effect of metabolites on KGD (SSA dehydrogenase coupled assay). Metabolites were used at 5 mM, except for acetyl-CoA (2 mM). Error bars represent the standard deviation from three independent experiments.

(D) Modulation of *Ms*KGD activity by different acyl-CoA analogs (0.2 mM) with respect to the control without ligands (S2AE: S-(2-acetamidoethyl)-ethanethioate). Error bars represent the standard deviation from three independent experiments. See also Figure S2.

for the observed inhibition, we determined the crystal structure of the shorter construct *Ms*KGD$_{\Delta 360}$ (comprising only the catalytic core) at 1.96 Å resolution (Table 1). However, the comparison of the *Ms*KGD$_{\Delta 360}$ and *Ms*KGD$_{\Delta 115}$ structures revealed that the catalytic core was essentially invariant upon deletion of the N-terminal domain (Figure S1D), suggesting that enzyme inhibition results from changes in dynamic—rather than structural—properties of the protein (see below).

The low basal activity of full-length KGD (Figure 2B) suggests that the enzyme might require stimulation by specific activator molecule(s) to achieve full activity in vivo. To test this hypothesis, we searched for possible enzyme modulators among various metabolic intermediates from the TCA cycle and glutamate biosynthetic pathways. This screening revealed that KGD activity was significantly higher in the presence of acetyl-CoA, the main substrate of the TCA cycle (Figure 2C). Acetyl-CoA had no effect on *Ec*SucA, but it activated all *Ms*KGD constructs and particularly the full-length enzyme, for which it largely compensates the inhibitory effect of the acyltransferase-like domain (Figure 2B). Furthermore, the combined effect of the two KGD regulators, acetyl-CoA and GarA, is additive (Figure 2B) and depends on their respective concentrations, suggesting that these molecules bind to independent regulatory sites in the catalytic core of *Ms*KGD.

Different adenine nucleotides are known to modulate bacterial and eukaryotic KDH activity (Bunik and Strumilo, 2009), and the structure of the *Ec*SucA homolog revealed the presence of an AMP-binding pocket situated away from the catalytic center (Frank et al., 2007). However, *Ms*KGD stimulation is highly specific for acetyl-CoA. Both the phosphoadenosine and acetyl moieties of the ligand are important for activation because neither CoA nor the synthetic compound S-(2-acetamidoethyl)-ethanethioate (which mimics the terminal acetyl-phosphopantetheine group of acetyl-CoA) has an activation effect (Figure 2D). Furthermore, other related acyl-CoA molecules are not only poorer activators when assayed at similar ligand: enzyme molar ratios (Figure 2D), but they are also found at much lower physiological concentrations (Chohnan et al., 1997).

KDH Activity in Mycobacteria

The unforeseen requirement for acetyl-CoA activation and the structural and functional similarities of *Ms*KGD with *Ec*SucA led us to reassess the apparently missing KDH activity in mycobacteria (Tian et al., 2005b). Reconstitution of the equivalent *M. smegmatis* complex in vitro using *Ms*KGD (E1o), DlaT (E2o), and Lpd (E3o) revealed a significant activity leading to the production of succinyl-CoA from KG and CoA, with reduction of NAD^+ (Figure 2A). As shown in Figure S2, matching functional properties were also observed for Rv1248c, the *Mtb* KGD homolog. Furthermore, KDH activity was stimulated by acetyl-CoA and inhibited by GarA in both *M. smegmatis* and *Mtb* KDH complexes, and the presence of glyoxylate did not abolish dehydrogenase (or decarboxylase) activities (Figure S2). As a crucial control, KDH activity could also be measured in wild-type *M. smegmatis* cell extracts (specific activity of 0.42 ± 0.04 nmol of NADH analog/min/mg of total protein); this activity increased 3.5-fold in presence of 300 μM acetyl-CoA (1.46 ± 0.02 nmol NADH/min/mg) and was abolished in presence of 10 μM GarA. In contrast no KDH activity was detected under any of the aforementioned conditions in a *kgd* null mutant *M. smegmatis* strain, demonstrating that *Ms*KGD is part of a functional KDH complex in mycobacteria. Interestingly, the mycobacterial protein DlaT (carrying the lipoyl domains) is engaged in both KDH and PDH reactions (Tian et al., 2005b), suggesting that the mycobacterial KDH complex may exist as

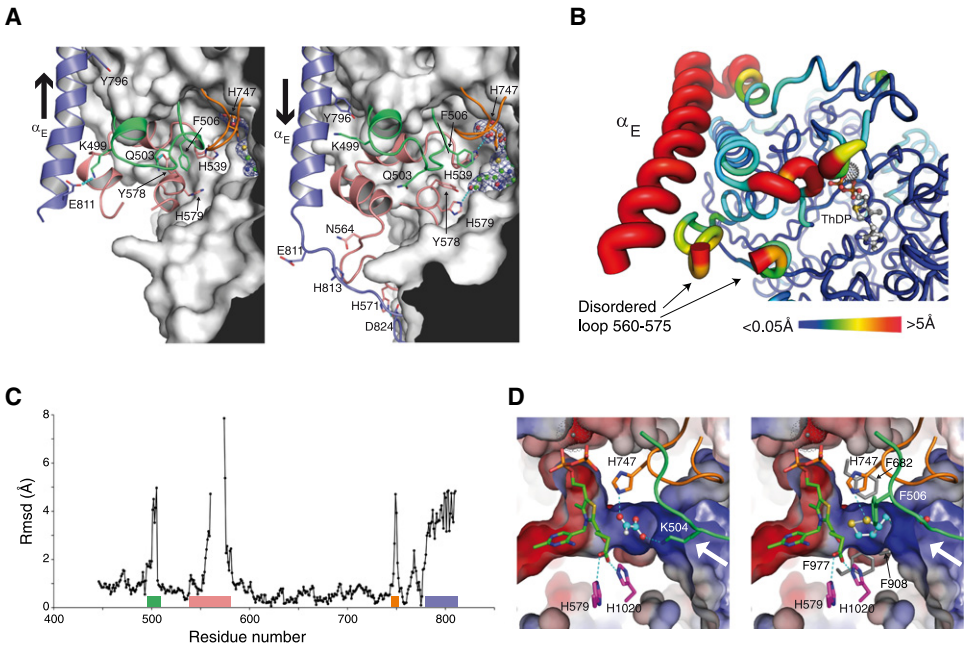

Figure 3. Formation of the Enamine-ThDP Intermediate Involves a Significant Structural Reorganization of the Active Site

(A) Structures of the substrate-free enzyme (left) and the enamine-ThDP intermediate (right). Structurally invariant regions of the protein are represented by their molecular surface, and loops that undergo significant movement are shown in cartoon representation. Selected side chains are shown explicitly in both panels.

(B) Structural comparison of the two proteins in (A) illustrating the large conformational changes in the vicinity of the active site.

(C) Root-mean-square deviations of equivalent Cα atoms from the first α/β domain (residues 446–810). Colored bars correspond to the loops shown in (A).

(D) Docking of the acceptor substrates glyoxylate (left panel, cyan) and lipoate (right panel, cyan) correctly oriented for catalysis in the entry channel (white arrows) that is generated by structuring of the loop 560–575 in the enamine-ThDP intermediate.

a mixed KDH/PDH complex. The presence of a similar hybrid complex was indeed reported for *C. glutamicum*, where it is further supported by copurification experiments (Niebisch et al., 2006) and deletion mutants of the DlaT homolog, AceF (Hoffelder et al., 2010). Therefore, the ability of mycobacterial KGD to sense the intracellular pool of acetyl-CoA, which is produced by PDH, may be important in coordinating the activities of the multienzyme aggregate.

Formation of the KDH complex requires the association between the E1o and E2o subunits. In mycobacteria, protein-protein interactions between KGD and DlaT are weak enough to prevent copurification ((Tian et al., 2005b; unpublished data). Nevertheless, a shorter *Ms*KGD construct devoid of its N-terminal region (*Ms*KGD$_{\Delta 360}$) was unable to sustain KDH activity (Figure 2A), and similar observations have been reported for N-terminal truncations of *Ec*SucA (Frank et al., 2007) and *C. glutamicum* OdhA (Hoffelder et al., 2010), indicating the involvement of the N-terminal region of E1o in protein-protein interactions. In particular a highly conserved motif with a predicted helical structure has been identified near the N terminus in both SucA and KGD/OdhA homologs, suggesting that it could play an important role in KDH complex formation (Hoffelder et al., 2010). As noted by these authors, the KGD protein from *Mtb* (Rv1248c), as annotated in databases and used by Tian et al. (2005b), lacks the first ten residues of this consensus sequence, which might account in part for their reported lack of KDH activity.

Protein Motions during Catalysis Generate the Acceptor Substrate-Binding Site

The three enzymatic activities measured for *Ms*KGD share a first common step, which is highly specific for KG (de Carvalho et al., 2010; Tian et al., 2005a) and involves the attack of the ThDP ylid on the substrate to form the ThDP α-carbanion/enamine intermediate upon decarboxylation. To gain further structural insight into substrate specificity and regulation mechanisms, we determined the crystal structure of this intermediate at 2.25 Å resolution (Table 1) using cryotrapping techniques. The structural comparison with the substrate-free enzyme revealed significant conformational changes taking place in the active site during catalysis (Figure 3A). The hydroxy-carboxyethylidene-ThDP adduct is well defined in the electron density map, and is maintained in the right conformation for catalysis through ionic interactions between its carboxylate group and the imidazole groups of His579 and His1020. The engagement of His579 breaks the stacking interactions between Phe506 and Tyr578 in the apoenzyme, and forces His539 to make hydrogen-bonding interactions with the pyrophosphate group, ultimately promoting a significant structural rearrangement of the active site (Figures 3B and 3C). This overall reorganization includes the concerted movements of the helical hairpin 538–560, the external helix α_E (which moves 3.5 Å along its main axis), and the loops 495–508, 561–580, and 746–752, involving an extensive rearrangement of intramolecular hydrophobic and hydrogen-bonding interactions.

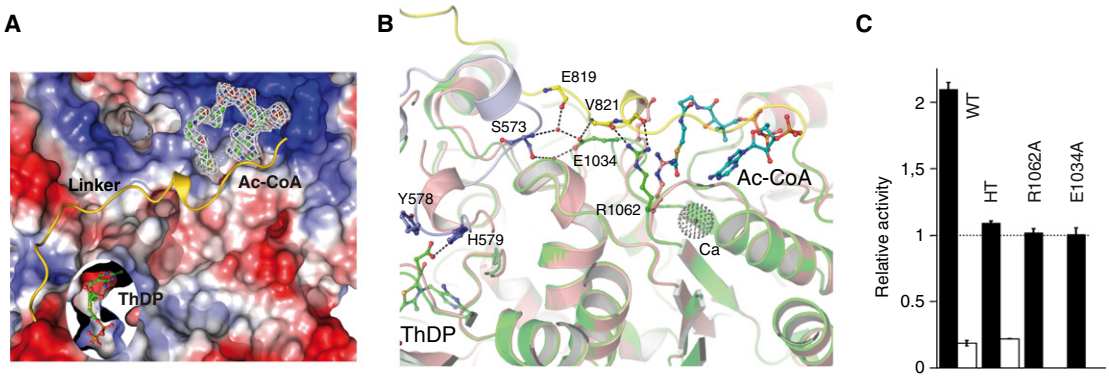

Figure 4. Structural Basis of acetyl-CoA Activation

(A) View of the ligand-binding site, with the interdomain linker shown in cartoon representation.

(B) Superposition of the substrate-free enzyme (pink) and the enamine-ThDP intermediate (green) bound to acetyl-CoA (cyan). The interdomain linker (yellow) and the loop 561–580 (blue) are shown as seen in the reaction intermediate because they are disordered in the substrate-free enzyme.

(C) Effect of GarA FHA (white bars) or acetyl-CoA (black bars) on the activities of wild-type *Ms*KGD$_{\Delta 360}$, the reconstituted heterotetramer (HT) *Ms*KGD$_{361–811}$ plus *Ms*KGD$_{830–1227}$ (lacking the linker segment), and the *Ms*KGD$_{\Delta 360}$ point mutants Arg1062-Ala and Glu1034-Ala. Error bars represent the standard deviation from three independent experiments.

These protein motions during catalysis can account for the partial inhibitory effect of the N-terminal acyltransferase-like domain on the catalytic core (Figure 2B). As mentioned above, the presence of the domain does not promote significant conformational changes in the ThDP-dependent active site (Figure S1D). Instead, the N-terminal domain directly interacts with the loop preceding the external helix α_E and could, therefore, interfere with the movement of this helix during catalysis, suggesting that the observed inhibition results from a dynamic effect. This hypothesis was experimentally confirmed by mutagenesis. The catalytic core residue Arg781, from the loop preceding helix α_E, is buried at the interface with the N-terminal domain (Figure S1C) and undergoes a significant movement (~4 Å; Figure 3C) during the catalytic cycle. Its guanidinium side chain forms a salt bridge with Glu715 and is engaged in hydrogen-bonding interactions with the main-chain carbonyl groups of Lys148, Arg149, and Thr150 from the N-terminal domain. Abrogation of these interactions by the Arg781-Ala substitution in *Ms*KGD$_{\Delta 115}$ significantly enhanced the catalytic activity of the protein, from 38.8 ± 0.6 to 173.4 ± 3.9 nmol of NADPH product/min/mg, a value similar to that measured for *Ms*KGD$_{\Delta 360}$ (161.0 ± 5.0 nmol of NADPH product/min/mg, as shown in Figure 2B). These observations indicate that the intersubunit interactions of the guanidinium side chain are largely responsible for the dynamic restraints imposed by the presence of the additional domain on full-length *Ms*KGD.

Another major consequence of the structural transition during catalysis involves a disorder-to-order transition of the active site loop 561–580 and the interdomain linker after helix α_E (residues 810–830), both of which were disordered in the substrate-free enzyme. In contrast these two loops adopt well-defined conformations in the enamine-ThDP reaction intermediate (Figure 3A, right panel), where they interact with each other and generate the binding site for the acceptor substrate(s). Manual docking of glyoxylate or the oxidized lipoate group, correctly oriented for catalysis within this active site entry channel (Figure 3D), suggests that His747 is well positioned to support the transfer reaction. Furthermore, the positively charged side chain of Lys504 (at a position largely conserved in SucA/KGD homologs) might form salt bridge interactions with the carboxylate group of glyoxylate, whereas four invariant phenylalanine residues (at *Ms*KGD positions 506, 682, 908, and 977) provide a hydrophobic environment for the lipoate group. The reaction of the enamine-ThDP intermediate with the acceptor substrate(s) represents the rate-limiting step (Graham et al., 1989) and will determine the final outcome of catalysis, depending on the nature (proton, lipoate group, or glyoxylate), enzyme-binding affinities, and physiological concentrations of the different acceptor substrate(s).

Structural Basis for Acetyl-CoA Activation

The structures of the *Ms*KGD$_{\Delta 360}$ and the enamine-ThDP intermediate in complex with acetyl-CoA were determined at 2.2 and 2.4 Å resolution, respectively, after rapid soaking and freezing of the crystals (Table 1). The ligand occupies a shallow allosteric pocket ~40 Å away from the catalytic site (Figure 4A), and the binding site is primarily defined by residues from the C-terminal α/β domain of the *Ms*KGD subunit, where the phosphate groups of acetyl-CoA interact with a positively charged region of the protein surface. A structural link between this allosteric site and the crucial active site loop 561–580 is provided by the interdomain linker (residues 810–830), which tracks along the molecular surface in the structure of the enamine-ThDP intermediate (Figure 4A) but is disordered in the substrate-free enzyme. As part of the structural transition during catalysis, two amino acid side chains close to the allosteric acetyl-CoA-binding site (Arg1062 and Glu1034) reorient to get engaged in direct and water-mediated hydrogen bonding interactions with residues Glu819, Val821, and Glu822 from the linker and Ser573 from the active site loop 560–580 (Figure 4B). Binding of acetyl-CoA to the substrate-free enzyme was seen to promote analogous structural changes of the Arg1062 and Glu1034 side chains, anticipating part of the protein motions required for catalysis and suggesting, therefore, a possible mechanism of activation.

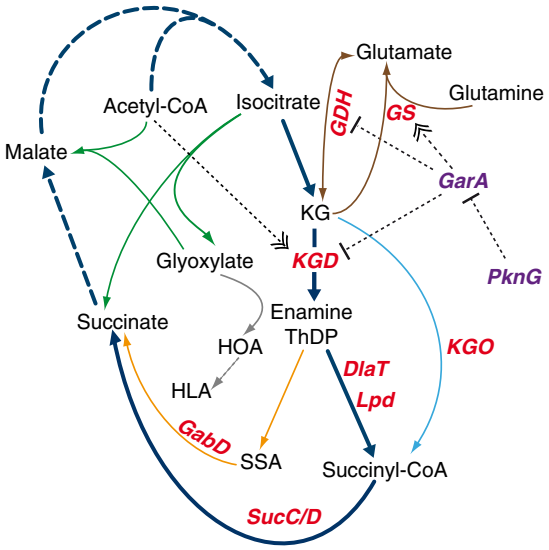

Figure 5. Alternative TCA Cycles in Mycobacteria

The three different pathways to convert KG into succinate and known elements of regulation (acetyl-CoA, GarA-PknG) are shown. The additional reactions of KG regulated by GarA-PknG are also indicated. Pathways shown are the standard TCA cycle (thick blue), glutamate metabolism (brown), glyoxylate shunt (green), and the two alternative ways to convert KG into succinate, via KGO (light blue) and SSA (orange). Reaction substrates and products are shown in black, and enzyme names are shown in red (GDH, glutamate dehydrogenase; GS, glutamate synthase; KGO, KG oxidoreductase; SucC/D, succinyl-CoA synthetase; GabD, SSA dehydrogenase; DlaT, dihydrolipoamide transferase; Lpd, lipoamide dehydrogenase).

In agreement with this interpretation, the structure of the enamine-ThDP intermediate remained essentially invariant upon binding of acetyl-CoA, and the entire ligand was clearly visible in the electron density map (Figure 4A). In contrast, part of the phosphopantetheine moiety of acetyl-CoA and the interdomain linker were disordered in the complex with the substrate-free enzyme, presumably because the full structural transition cannot be achieved in the absence of substrate. Alternatively, but not exclusively, crystal contacts might prevent significant protein motions to take place because longer soaking times of acetyl-CoA in *Ms*KGD$_{\Delta 360}$ crystals led to severe loss of diffraction.

The activation mechanism suggested by the crystal structures, implying a major role for the interdomain linker 810–830, was further confirmed by mutagenesis. A heterotetrameric construct in which this linker was omitted (i.e., separating the enzyme into two polypeptides, as in other heterotetrameric 2-oxoacid dehydrogenases) retained both KGD activity and GarA inhibition but was significantly impaired for acetyl-CoA-dependent activation (Figure 4C). The differential properties of this construct, which is inhibited by GarA but is not stimulated by acetyl-CoA, demonstrate that the two regulators bind to distinct, independent target sites in the catalytic core of the protein, thus accounting for their additive effect on *Ms*KGD activity (Figure 2B). Further validation of the proposed activation mechanism is provided by the alanine substitution of either Arg1062 or Glu1034, which are predicted to mediate acetyl-CoA-induced stimulation (Figure 4B). These point mutations did not affect the specific activity of the wild-type protein but completely abolished activation (Figure 4C), validating the hypothesis that the local changes induced by acetyl-CoA binding contribute to lowering the activation energy barrier for the first reaction step.

SIGNIFICANCE

Our structural and biochemical results unambiguously demonstrate that bacterial E1o homologs, including mycobacterial KGD and *Ec*SucA, share similar multifunctional properties, capable of sustaining KG dehydrogenase (succinyl-transferring, EC1.2.4.2), KG decarboxylase (EC 4.1.1.71), and 2-hydroxy-3-oxoadipate synthase (EC 2.2.1.5) activities. The first two reactions provide alternative pathways for the TCA cycle to work in a cyclic mode for energy production, whereas the carboligase reaction might detoxify the cell from high glyoxylate concentrations, or alternatively serve for the generation of biosynthetic precursors (de Carvalho et al., 2010). Although further studies are required to investigate the physiological implications of these findings, the expression of an anaerobic-like KG:ferredoxin oxidoreductase (KGO) in *M. tuberculosis* (Baughn et al., 2009) and a multifunctional KGD functioning either as KG decarboxylase (de Carvalho et al., 2010; Tian et al., 2005a) or dehydrogenase (as shown here) provide three alternative pathways to link the oxidative and reductive branches of the TCA cycle (Figure 5). All these pathways are functional in intermediary metabolism because *M. tuberculosis* strains lacking KGO or KGD displayed wild-type-like growth phenotypes on either carbohydrates (*Δkgo*) or exogenous fatty acids (*Δkgd*) as the carbon source, whereas the double-mutant *Δkgo Δkgd* strain was strictly dependent on the glyoxylate shunt (Baughn et al., 2009). These alternative functional modes of the TCA cycle as well as the unique regulatory properties of mycobacterial KGD, under the allosteric control of metabolic (acetyl-CoA) and phospho-dependent (GarA) regulators (Figure 5), can endow *M. tuberculosis* with the metabolic plasticity required for growth on diverse host-derived carbon sources, and appeal for further investigation to ascertain the full physiological implications of these findings.

EXPERIMENTAL PROCEDURES

Cloning and Mutagenesis

Genes were amplified by PCR from genomic DNA of *M. smegmatis* mc^2 155 (MSMEG_5049 for *kgd*, MSMEG_3647 for *garA*, MSMEG_4283 for *dlaT*, and MSMEG_0903 for *lpd*), *Mtb* H37Rv (Rv0243c for *gabD1*, Rv1248c for *kgd*), and *E. coli* DH5α (*sucA*, *sucB*, *lpd*). All genes were cloned in pET-28a (Novagen) by standard techniques. Site-directed mutagenesis of *Ms*KGD was performed by PCR on pET28a-*Ms*KGD$_{\Delta 360}$. All plasmids were verified by DNA sequencing.

Protein Production and Purification

Full-length *M. smegmatis* GarA and its FHA domain (GarA$_{\Delta 44}$) were expressed in *E. coli* BL21AI, transformed with the appropriate expression plasmid (pET-28a/*garA* or pET-28a/FHA), and grown in fed-batch mode into a 1l BIOSTAT Q™ Fermentor unit (Sartorius), in glycerol media supplemented with 0.1% glucose optimized from published conditions (Pinsach et al., 2006). Expression was induced by the addition of 0.2% arabinose and 1 mM IPTG for

11 hr at 23°C. The recombinant proteins were purified by Ni^{2+}-IMAC followed by size exclusion chromatography (SEC).

*Ms*KGD, its derivate mutants, *M. smegmatis* and *E. coli* Lpd, *Mtb* GabD1, *E. coli* SucB were expressed in *E. coli* BL21(DE3)pLysS, grown in LB media containing 50 μg/ml kanamycin and 34 μg/ml chloramphenicol (supplemented with 50 μM lipoic acid for *E. coli* SucB, 50 μM riboflavin for Lpd), and induced with 0.5 mM IPTG at 14°C for 20 hr. *Ec*SucA and *M. smegmatis* DlaT were expressed in the same strain, but induction was carried out for 3 hr at 30°C with 1 mM IPTG. All recombinant proteins were purified following a similar protocol. Fractions from Ni^{2+}-IMAC on HisTrap columns (GE Healthcare), containing the protein of interest as checked by SDS-PAGE, were dialyzed against 25 mM Tris-HCl (pH 7.6), 150 mM NaCl, 1 mM DTT, except for all constructions of $MsKGD_{\Delta 360}$ and *M. smegmatis* Lpd, for which the NaCl concentration was kept at 500 mM throughout. The N-terminal His_6 tag was removed by incubation for 12 hr at 18°C in the presence of His_6-tagged TEV protease (van den Berg et al., 2006) at a 1:30 ratio (w/w), followed by gravity-flow separation on Ni-NTA agarose (QIAGEN). SEC was performed on a Superdex 200 26/60 column (GE Healthcare) for most proteins, except for full-length *Ms*KGD, *M. smegmatis* DlaT, and *E. coli* SucB (run on a Sephacryl S400 column; GE Healthcare), and *M. smegmatis* GarA and GabD1 (run on a Sepharose 75 26/60; GE Healthcare). Fractions containing the eluted protein of interest were systematically checked on SDS-PAGE for purity >95% (as estimated by Coomassie blue staining), concentrated with Vivaspin units (Sartorius), and stored at −80°C after flash-freezing in liquid nitrogen.

A *Ms*KGD heterotetrameric mutant lacking the loop 810–830 was obtained from two coexpressed fragments, corresponding to residues Asp361-Leu810 (expressed from a gene fragment cloned in pET-28a) and residues Lys830-Gly1227 (fragment cloned in pET-23a). Expression and purification were carried out as described above. For functional assays the enzyme was reconstituted in vitro from SEC peaks containing the N-terminal and C-terminal fragments. The concentration of each purified protein was calculated from absorbance at λ = 280 nm, with the exception of *Ec*Lpd and *Ms*Lpd, whose concentrations were estimated by absorbance at both 280 and 446 nm to account for the absorbance from the bound FAD cofactor ($\varepsilon_{FAD446nm}$ = 11300 M^{-1}. cm^{-1}; $\varepsilon_{FAD280nm}$ = 21200 M^{-1}. cm^{-1}).

Enzyme Assays

For the determination of KGD activity, reactions contained 2 μM enzyme, 1–3 mM KG, 0.2 mM ThDP, 1 mM $MgCl_2$, 550–1100 nM GabD1, and 1–2 mM $NADP^+$ in 50 mM potassium phosphate (pH 6.5). Reactions were started by the addition of KG at 37°C, and initial rates were calculated during the linear phase of the reaction (10–20 min). When appropriate, GarA was diluted in PBS and added to the assay mixture at 5 μM unless otherwise stated. Experiments were performed in triplicate.

To determine the KDH activity, reactions contained 1–3 mM KG, 1 mM CoA-SH, 0.2 mM ThDP, 1 mM $MgCl_2$, 2 μM of *Ms*KGD/*Ec*SucA, 4 μM of *Ms*DlaT/*Ec*SucB, 0.5 μM of *Ms*Lpd/*Ec*Lpd, and 1–2 mM 3-acetylpyridine dinucleotide (AcNAD) in 50 mM potassium phosphate (pH 6.5). AcNAD was used instead of NAD^+ in order to prevent enzyme inhibition by NADH (Marco and Marco, 1974). Reactions were started by the addition of KG and were incubated at 37°C, and initial rates were calculated during the linear phase of the reaction (10–20 min). When required, GarA was diluted in PBS and added to a final concentration ranging from 0.02 to 10 μM, and acetyl-CoA to a final concentration ranging from 0.01 to 4 mM. The rate of AcNAD reduction was calculated by spectrophotometry based on the absorption coefficient of AcNADH (ε_{340nm} = 6220 M^{-1}. cm^{-1}). Each experiment was done in triplicate.

To detect SSA formation, reactions contained 1 mM KG, 0.1 mM ThDP, 1 mM $MgCl_2$, and 2 μM enzyme (*Ms*KGD, $MsKGD_{\Delta 360}$, Rv1248c, or *Ec*SucA) in 50 mM potassium phosphate (pH 6.5) (0.5 ml), and were incubated for 1 hr at 37°C. Control reactions lacked ThDP and $MgCl_2$ and contained 5 μM $GarA_{\Delta 44}$. Reaction products were derivatized with 2,4-dinitrophenylhydrazine and separated by thin-layer chromatography as described (Tian et al., 2005a).

Analysis of Reaction Products by Mass Spectrometry

Reactions were set up as above but contained additional DlaT (4 μM), Lpd (0.5 μM), CoA-SH (1 mM), acetyl-CoA (0.1 mM), and AcNAD (1 mM), with or without glyoxylate (1 mM). After incubation at 37°C for 1 hr, GabD1 (1 μM) and $NADP^+$ (1 mM) were added for 15 min to convert SSA to succinate. Reaction products were analyzed by LC-MS using a Xevo QTof mass spectrometer (Waters) coupled to an Acquity LC system (Waters) using an Acquity UPLC BEH C18 column (2.1 × 50 mm; Waters). The flow rate was 0.6 ml/min^{-1}, and the gradient was as follows: 95% solvent A (0.1% formic acid in water) with 5% solvent B (0.1% formic acid in acetonitrile) was held constant for 0.5 min, then there was a linear gradient to 100% B over the next 2.1 min. After 1 min at 100% solvent B, the gradient was returned to 95% solvent A and 5% solvent B over 0.2 min. Mass accuracy was achieved using a reference lock mass scan, once per second. The ES cone voltage was 30 V, and collision energy was 4 eV. The MS acquisition rate was 10 spectra per second, and *m/z* data ranging from 50 to 1000 Da were collected.

M. smegmatis Gene Deletion, Cell Culture, and KDH Activity

The gene encoding *Ms*KGD in *M. smegmatis* mc^2 155 was replaced by an interrupted allele containing a kanamycin-resistance cassette by allelic exchange (Pelicic et al., 1997). Gene deletion was confirmed by PCR. The growth-deficient phenotype of the deletion strain was verified by complementation with plasmid-borne *Ms*KGD. Wild-type and *kgd* null strains were grown in 7H9 Middlebrook medium. To assess the KDH activity of cell extracts, reactions contained 0.6 mg/ml total protein, 1 mM CoA-SH, and 1 mM AcNAD, 0/3 mM KG in 50 mM potassium phosphate (pH 6.5). Reactions were started by addition of KG and incubated at 37°C for 20 min.

X-ray Crystallography and Structural Analysis

Initial crystallization screenings were carried out at 18°C by the vapor diffusion method using a Cartesian nanoliter dispensing system; hits were improved by handmade hanging drops in 24-well plates at the same temperature. Optimized conditions for crystal growth of $MsKGD_{\Delta 115}$ and $MsKGD_{\Delta 360}$ (20–25 mg/ml, supplemented with 2 mM ThDP and 5 mM $MgCl_2$) are as follows: $MsKGD_{\Delta 360}$: 46.5% MPD, 100 mM HEPES (pH 7.0); $MsKGD_{\Delta 115}$: 39% MPD, 100 mM HEPES (pH 7.0), 200 mM NaCl. The enamine-ThDP intermediate was trapped by flash-freezing $MsKGD_{\Delta 360}$ crystals (grown in 52% MPD, 20 mM sodium acetate, 5% 1,3-propanediol) equilibrated at 4°C and soaked with 20 mM KG for 2–6 min. To obtain the complexes with acetyl-CoA, $MsKGD_{\Delta 360}$ crystals were soaked either in mother liquor supplemented with 20 mM acetyl-CoA for 4 min at 18°C prior to freezing, or in mother liquor supplemented with 20 mM acetyl-CoA for 5 min at 4°C before adding 5 mM acetyl-CoA plus 25 mM KG for 1.5 min prior to freezing.

All diffraction data sets were collected from single crystals at 100 K using synchrotron radiation at the ESRF (Grenoble, France), SOLEIL (Saint-Aubin, France), or SLS (Villigen, Switzerland) (Table 1). Data were processed with either XDS (Kabsch, 2010) or iMosflm (Leslie, 2009) and scaled with XSCALE from the XDS package or SCALA from the CCP4 suite (CCP4, 1994). The crystal structure of $MsKGD_{\Delta 360}$ was solved by molecular replacement methods using the program AMoRe (Trapani and Navaza, 2008) and the homologous model of *Ec*SucA (PDB entry 2JGD) as the search model. The structure was refined with REFMAC5 (Murshudov et al., 1997) alternated with manual rebuilding with Coot (Emsley et al., 2010), and used to solve the other crystal structures by molecular replacement. The N-terminal acyltransferase-like domain could be manually traced from sigma A-weighted Fourier difference maps. All models were further refined with BUSTER (Bricogne et al., 2009) applying local structure similarity restraints for NCS and a TLS model, and validated with the MolProbity server (http://molprobity.biochem.duke.edu; Davis et al., 2007). Data collection and refinement statistics are reported in Table 1. Graphic figures and manual docking of the acceptor substrates were generated and rendered with PyMOL (DeLano, 2002).

ACCESSION NUMBERS

Crystallographic coordinates and structure factors were deposited in the Protein Data Bank with accession codes 2YIC ($MsKGD_{\Delta 360}$), 2XT6 ($MsKGD_{\Delta 115}$), 2YID (enamine-ThDP intermediate), 2XTA ($MsKGD_{\Delta 360}$-acetyl-CoA complex), and 2Y0P (enamine-ThDP intermediate in complex with acetyl-CoA).

SUPPLEMENTAL INFORMATION

Supplemental Information includes two figures and one table and can be found with this article online at doi:10.1016/j.chembiol.2011.06.004.

ACKNOWLEDGMENTS

We thank S.T. Cole for comments, P. Weber and A. Haouz for performing robot-driven crystallization trials, J. D'Alayer for protein sequencing, and G. Eaton for performing LC-MS. S-(2-acetamidoethyl)-ethanethioate was a gift by C. Vergne (CEA/Genoscope, Evry, France); the expression plasmid for TEV protease was provided by H. Berglund (Karolinska Institute, Stockholm, Sweden). We also thank ESRF, SOLEIL, and SLS for provision of synchrotron radiation facilities and their staffs for assistance in using the beamlines. This research was supported by grants from the European Union FP6 Project NM4TB (contract LSHP-CT-2005-018923), Agence Nationale de la Recherche (ANR, France, contracts ANR-08-MIEN-029-03 and ANR-09-BLAN-0400-01), a European Reintegration Grant (230874), a Royal Society Research Grant (UK), Institut Pasteur, and CNRS (France).

Received: March 28, 2011
Revised: May 24, 2011
Accepted: June 7, 2011
Published: August 25, 2011

REFERENCES

Baughn, A.D., Garforth, S.J., Vilchèze, C., and Jacobs, W.R., Jr. (2009). An anaerobic-type alpha-ketoglutarate ferredoxin oxidoreductase completes the oxidative tricarboxylic acid cycle of *Mycobacterium tuberculosis*. PLoS Pathog. *5*, e1000662.

Bott, M. (2007). Offering surprises: TCA cycle regulation in *Corynebacterium glutamicum*. Trends Microbiol. *15*, 417–425.

Bricogne, G., Blanc, E., Brandl, M., Flensburg, C., Keller, P., Paciorek, W., Roversi, P., Smart, O.S., Vonrhein, C., and Womack, T.O. (2009). BUSTER, version 2.9.3 (Cambridge: Global Phasing Ltd).

Bunik, V.I., and Fernie, A.R. (2009). Metabolic control exerted by the 2-oxoglutarate dehydrogenase reaction: a cross-kingdom comparison of the crossroad between energy production and nitrogen assimilation. Biochem. J. *422*, 405–421.

Bunik, V.I., and Strumilo, S. (2009). Regulation of catalysis within cellular network: metabolic and signaling implications of the 2-oxoglutarate oxidative decarboxylation. Curr. Chem. Biol. *3*, 279–290.

CCP4 (Collaborative Computational Project, Number 4). (1994). The CCP4 suite: programs for protein crystallography. Acta Crystallogr. D Biol. Crystallogr. *50*, 760–763.

Chohnan, S., Furukawa, H., Fujio, T., Nishihara, H., and Takamura, Y. (1997). Changes in the size and composition of intracellular pools of nonesterified coenzyme A and coenzyme A thioesters in aerobic and facultatively anaerobic bacteria. Appl. Environ. Microbiol. *63*, 553–560.

Cole, S.T., Brosch, R., Parkhill, J., Garnier, T., Churcher, C., Harris, D., Gordon, S.V., Eiglmeier, K., Gas, S., Barry, C.E., 3rd., et al. (1998). Deciphering the biology of *Mycobacterium tuberculosis* from the complete genome sequence. Nature *393*, 537–544.

Davis, I.W., Leaver-Fay, A., Chen, V.B., Block, J.N., Kapral, G.J., Wang, X., Murray, L.W., Arendall, W.B., 3rd, Snoeyink, J., Richardson, J.S., and Richardson, D.C. (2007). MolProbity: all-atom contacts and structure validation for proteins and nucleic acids. Nucleic Acids Res. *35* (Web Server issue), W375–W383.

de Carvalho, L.P., Zhao, H., Dickinson, C.E., Arango, N.M., Lima, C.D., Fischer, S.M., Ouerfelli, O., Nathan, C., and Rhee, K.Y. (2010). Activity-based metabolomic profiling of enzymatic function: identification of Rv1248c as a mycobacterial 2-hydroxy-3-oxoadipate synthase. Chem. Biol. *17*, 323–332.

DeLano, W.L. (2002). The PyMOL Molecular Graphics System (Palo Alto, CA: DeLano Scientific).

Emsley, P., Lohkamp, B., Scott, W.G., and Cowtan, K. (2010). Features and development of Coot. Acta Crystallogr. D Biol. Crystallogr. *66*, 486–501.

Frank, R.A., Price, A.J., Northrop, F.D., Perham, R.N., and Luisi, B.F. (2007). Crystal structure of the E1 component of the *Escherichia coli* 2-oxoglutarate dehydrogenase multienzyme complex. J. Mol. Biol. *368*, 639–651.

Graham, L.D., Packman, L.C., and Perham, R.N. (1989). Kinetics and specificity of reductive acylation of lipoyl domains from 2-oxo acid dehydrogenase multienzyme complexes. Biochemistry *28*, 1574–1581.

Guest, J.R. (1995). The Leeuwenhoek Lecture, 1995. Adaptation to life without oxygen. Philos. Trans. R. Soc. Lond. B Biol. Sci. *350*, 189–202.

Hoffelder, M., Raasch, K., van Ooyen, J., and Eggeling, L. (2010). The E2 domain of OdhA of *Corynebacterium glutamicum* has succinyltransferase activity dependent on lipoyl residues of the acetyltransferase AceF. J. Bacteriol. *192*, 5203–5211.

Kabsch, W. (2010). Xds. Acta Crystallogr. D Biol. Crystallogr. *66*, 125–132.

Keevil, C.W., Hough, J.S., and Cole, J.A. (1979). Regulation of 2-oxoglutarate dehydrogenase synthesis in *Citrobacter freundii* by traces of oxygen in commercial nitrogen gas and by glutamate. J. Gen. Microbiol. *114*, 355–359.

Knapp, J.E., Carroll, D., Lawson, J.E., Ernst, S.R., Reed, L.J., and Hackert, M.L. (2000). Expression, purification, and structural analysis of the trimeric form of the catalytic domain of the *Escherichia coli* dihydrolipoamide succinyltransferase. Protein Sci. *9*, 37–48.

Krawczyk, S., Raasch, K., Schultz, C., Hoffelder, M., Eggeling, L., and Bott, M. (2010). The FHA domain of OdhI interacts with the carboxyterminal 2-oxoglutarate dehydrogenase domain of OdhA in *Corynebacterium glutamicum*. FEBS Lett. *584*, 1463–1468.

Leslie, A.G.W. (2009). iMosflm, version 1.0.4 (computer program) (Cambridge: MRC-LMB).

Lindqvist, Y., Schneider, G., Ermler, U., and Sundström, M. (1992). Three-dimensional structure of transketolase, a thiamine diphosphate dependent enzyme, at 2.5 A resolution. EMBO J. *11*, 2373–2379.

Marco, E.J., and Marco, R. (1974). The use of 3-acetyl-pyridine adenine dinucleotide in the spectrophotometric assay of enzymatic activities coupled to dehydrogenases of unfavorable equilibrium. Anal. Biochem. *62*, 472–477.

McKinney, J.D., Höner zu Bentrup, K., Muñoz-Elías, E.J., Miczak, A., Chen, B., Chan, W.T., Swenson, D., Sacchettini, J.C., Jacobs, W.R., Jr., and Russell, D.G. (2000). Persistence of *Mycobacterium tuberculosis* in macrophages and mice requires the glyoxylate shunt enzyme isocitrate lyase. Nature *406*, 735–738.

Muller, Y.A., Lindqvist, Y., Furey, W., Schulz, G.E., Jordan, F., and Schneider, G. (1993). A thiamin diphosphate binding fold revealed by comparison of the crystal structures of transketolase, pyruvate oxidase and pyruvate decarboxylase. Structure *1*, 95–103.

Murshudov, G.N., Vagin, A.A., and Dodson, E.J. (1997). Refinement of macromolecular structures by the maximum-likelihood method. Acta Crystallogr. D Biol. Crystallogr. *53*, 240–255.

Murthy, P.S., Sirsi, M., and Ramakrishnan, T. (1962). Tricarboxylic acid cycle and related enzymes in cell-free extracts of *Mycobacterium tuberculosis* H37Rv. Biochem. J. *84*, 263–269.

Nemeria, N., Chakraborty, S., Baykal, A., Korotchkina, L.G., Patel, M.S., and Jordan, F. (2007). The 1′,4′-iminopyrimidine tautomer of thiamin diphosphate is poised for catalysis in asymmetric active centers on enzymes. Proc. Natl. Acad. Sci. USA *104*, 78–82.

Niebisch, A., Kabus, A., Schultz, C., Weil, B., and Bott, M. (2006). Corynebacterial protein kinase G controls 2-oxoglutarate dehydrogenase activity via the phosphorylation status of the OdhI protein. J. Biol. Chem. *281*, 12300–12307.

Nott, T.J., Kelly, G., Stach, L., Li, J., Westcott, S., Patel, D., Hunt, D.M., Howell, S., Buxton, R.S., O'Hare, H.M., and Smerdon, S.J. (2009). An intramolecular switch regulates phosphoindependent FHA domain interactions in *Mycobacterium tuberculosis*. Sci. Signal. *2*, ra12.

O'Fallon, J.V., and Brosemer, R.W. (1977). Cellular localization of alpha-ketoglutarate: glyoxylate carboligase in rat tissues. Biochim. Biophys. Acta *499*, 321–328.

O'Hare, H.M., Durán, R., Cerveñansky, C., Bellinzoni, M., Wehenkel, A.M., Pritsch, O., Obal, G., Baumgartner, J., Vialaret, J., Johnsson, K., and Alzari, P.M. (2008). Regulation of glutamate metabolism by protein kinases in mycobacteria. Mol. Microbiol. *70*, 1408–1423.

Pelicic, V., Jackson, M., Reyrat, J.M., Jacobs, W.R., Jr., Gicquel, B., and Guilhot, C. (1997). Efficient allelic exchange and transposon mutagenesis in *Mycobacterium tuberculosis*. Proc. Natl. Acad. Sci. USA *94*, 10955–10960.

Pinsach, J., de Mas, C., and López-Santin, J. (2006). A simple feedback control of *Escherichia coli* growth for recombinant aldolase production in fed-batch mode. Biochem. Eng. J. *29*, 235–242.

Pitson, S.M., Mendz, G.L., Srinivasan, S., and Hazell, S.L. (1999). The tricarboxylic acid cycle of *Helicobacter pylori*. Eur. J. Biochem. *260*, 258–267.

Schlossberg, M.A., Bloom, R.J., Richert, D.A., and Westerfeld, W.W. (1970). Carboligase activity of alpha-ketoglutarate dehydrogenase. Biochemistry *9*, 1148–1153.

Tian, J., Bryk, R., Itoh, M., Suematsu, M., and Nathan, C. (2005a). Variant tricarboxylic acid cycle in *Mycobacterium tuberculosis*: identification of alpha-ketoglutarate decarboxylase. Proc. Natl. Acad. Sci. USA *102*, 10670–10675.

Tian, J., Bryk, R., Shi, S., Erdjument-Bromage, H., Tempst, P., and Nathan, C. (2005b). *Mycobacterium tuberculosis* appears to lack alpha-ketoglutarate dehydrogenase and encodes pyruvate dehydrogenase in widely separated genes. Mol. Microbiol. *57*, 859–868.

Tomb, J.F., White, O., Kerlavage, A.R., Clayton, R.A., Sutton, G.G., Fleischmann, R.D., Ketchum, K.A., Klenk, H.P., Gill, S., Dougherty, B.A., et al. (1997). The complete genome sequence of the gastric pathogen *Helicobacter pylori*. Nature *388*, 539–547.

Trapani, S., and Navaza, J. (2008). AMoRe: classical and modern. Acta Crystallogr. D Biol. Crystallogr. *64*, 11–16.

Usuda, Y., Tujimoto, N., Abe, C., Asakura, Y., Kimura, E., Kawahara, Y., Kurahashi, O., and Matsui, H. (1996). Molecular cloning of the *Corynebacterium glutamicum* ('*Brevibacterium lactofermentum*' AJ12036) *odhA* gene encoding a novel type of 2-oxoglutarate dehydrogenase. Microbiology *142*, 3347–3354.

van den Berg, S., Löfdahl, P.A., Härd, T., and Berglund, H. (2006). Improved solubility of TEV protease by directed evolution. J. Biotechnol. *121*, 291–298.

Waskiewicz, D.E., and Hammes, G.G. (1984). Elementary steps in the reaction mechanism of the alpha-ketoglutarate dehydrogenase multienzyme complex from *Escherichia coli*: kinetics of succinylation and desuccinylation. Biochemistry *23*, 3136–3143.

Wayne, L.G., and Hayes, L.G. (1996). An *in vitro* model for sequential study of shiftdown of *Mycobacterium tuberculosis* through two stages of nonreplicating persistence. Infect. Immun. *64*, 2062–2069.

Yamasaki, H., and Moriyama, T. (1970). Alpha-ketoglutarate: glyoxylate carboligase activity in *Escherichia coli*. Biochem. Biophys. Res. Commun. *39*, 790–795.

Yamasaki, H., and Moriyama, T. (1971). Purification, general properties and two other catalytic activities of -ketoglutarate:glyoxylate carboligase of *Mycobacterium Phlei*. Biochim. Biophys. Acta *242*, 637–647.

